CHEMISTRY OF MATERIALS

Article

pubs.acs.org/cm

Microscale Controlled Electrogeneration of Patterned Mesoporous Silica Thin Films

Yann Guillemin, Mathieu Etienne, Emilie Sibottier, and Alain Walcarius*

Laboratoire de Chimie Physique et Microbiologie pour l'Environnement, UMR 7564, CNRS−Nancy University, 405 rue de Vandoeuvre, F-54600 Villers-lès-Nancy, France

S Supporting Information

ABSTRACT: Mesoporous and mesostructured thin films typically prepared through the combination of low cost sol−gel processing and supramolecular chemistry are important in a wide range of applications including micro-optics and photonic devices, microelectronics, sensors, energy, environment, coatings, biomaterials, and biomicrofluidics, among others. For many of them, the full practical exploitation of these high-tech materials requires the development of micro- and nanofabrication technologies. Even if some patterning techniques have been proposed for mesostructured films (often based on extension of established procedures to mesoporous materials), controlling the important features of the local deposits (e.g., pore orientation) is still challenging. Here, we describe a novel concept to locally generate surfactant-templated silica nanostructures using a scanning electrochemical microscope. The method is based on a fine nonelectrochemical positioning of an ultramicroelectrode close to a solid support immersed in a surfactant-containing hydrolyzed sol solution, the tip electrode being then used as a micrometric "pen" inducing self-assembly polycondensation of the precursors by local pH change under potential control. Tuning the characteristics of the deposits (size, thickness, structure) can be easily achieved by adjusting some key parameters (potential, distance to the surface, size of the electrode). It was notably shown that using the tip as the counter-electrode and the underlying support as the working electrode enabled to get vertically oriented mesopores in honeycomb-structured microdots (i.e., the most suitable configuration for diffusion-controlled applications), which cannot be obtained by other patterning techniques. The proof-of-concept of electrochemically driven nanolithography demonstrated here for silica should be applicable to other patterned mesostructures (other oxides or functionalized materials).

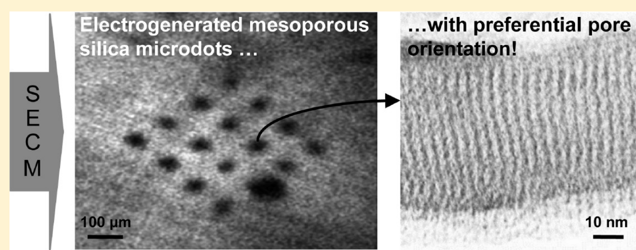

KEYWORDS: *mesoporous thin films, electrochemically assisted deposition, sol−gel, micropatterning, scanning electrochemical microscope, surfactant template, oriented porosity*

INTRODUCTION

Mesoporous and mesostructured materials prepared by bottom-up self-assembly of regular sol−gel networks around surfactant or polymer templates[1−4] are among the most attractive synthetic objects, exhibiting unprecedented properties in terms of porosity, structure and reactivity.[4−10] Though being manufactured in various forms,[4] the thin film configuration is highly recommended for several applications such as micro-optics and photonic devices, microelectronics, sensors, energy, environment, coatings, biomaterials, biomicrofluidics, among others.[11−16] Mesoporous films are typically prepared by sol−gel processing using primarily evaporation-induced self-assembly approaches associated to deposition by dip coating, spin coating, casting, or spraying.[14,17−21] Many examples of silica, metal oxide, and hybrid organic−inorganic films have been reported so far,[14] for which ordered mesophases can be obtained in distinct nanoscale morphologies (hexagonal, cubic, tetragonal, orthorhombic, bicontinuous, or less-ordered worm-like structures). Recent efforts have been focused on controlling mesopore orientation,[22−25] especially in a direction perpendicular to the underlying substrate,[26−34] or on generating thin films with multimodal porosity,[35,36] because these lead to optimal configurations ensuring highest accessibilities from the film surface.

The full practical exploitation of these high-tech materials requires however the development of micro- and nanofabrication technologies, especially for applications in the field of microelectronics, photonics, or chip-based sensing devices. Some patterning techniques have been proposed for mesostructured films. They are often based on extension of established procedures to mesoporous materials, including conventional and less conventional lithographic techniques as well as some other approaches[37] (UV patterning,[38,39] rapid prototyping by micropen lithography,[40] dip-pen nanolithography,[41] site-selective deposition on surfaces prepatterned with self-assembled monolayers,[42,43] electron-beam lithography,[44,45] inkjet printing,[46] or replication of micromolds, micropatterned surfaces or copolymer patterns.[47−49] Even if these methods can

Received: February 5, 2011
Revised: November 15, 2011
Published: November 16, 2011

 © 2011 American Chemical Society

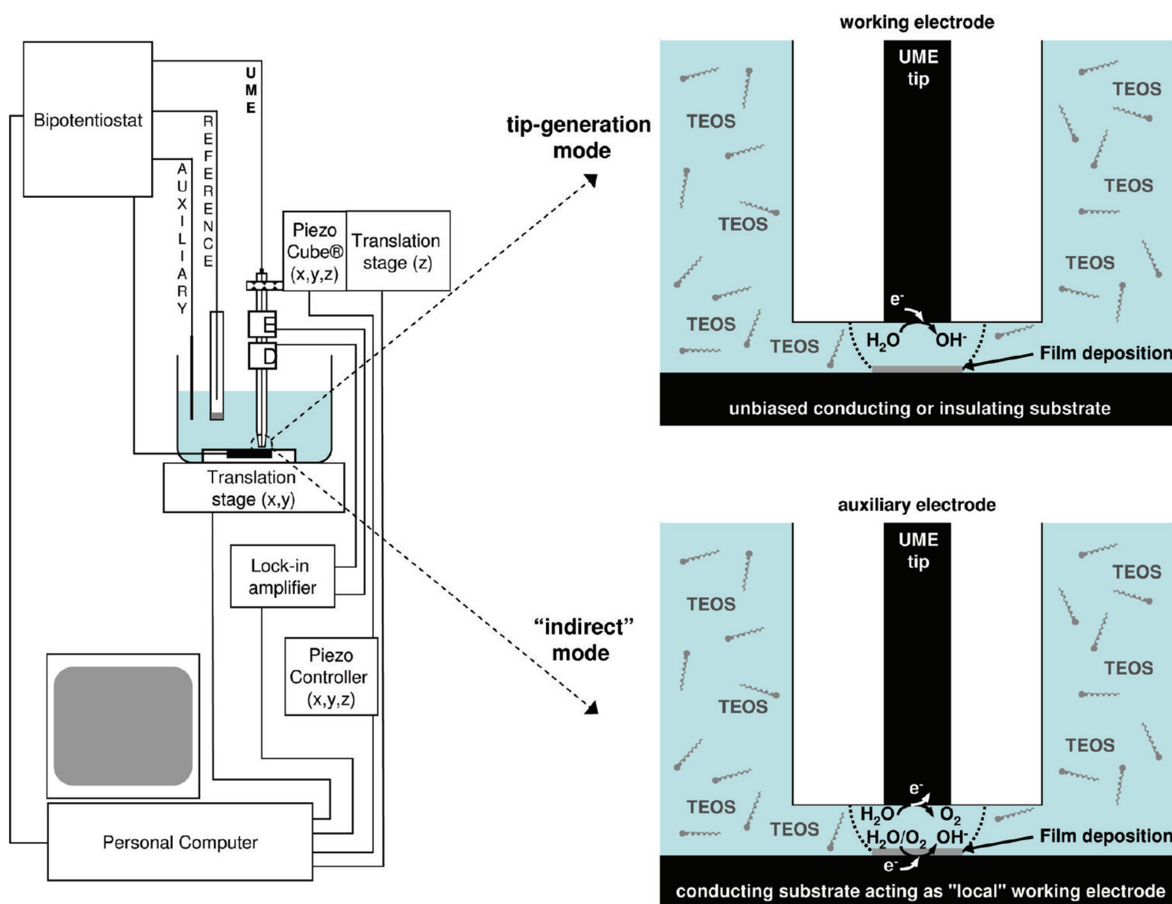

Figure 1. Schematic representation of the SECM device used to locally generate surfactant-templated mesoporous silica patterns. Left, schematic diagram of the SECM microscope. Right, expanded view of the UME−substrate region for both tip generation mode (top) and "indirect" mode (bottom), including redox reactions involved in the processes.

be effectively used to define patterns in mesoporous films, they are mostly restricted to flat surfaces only (except for aerosol writing[50]), and controlling the important features of local deposits (e.g., pore orientation) is still challenging. As mentioned in a recent review dealing with mesostructured films, the field is still largely unexplored and several new methods and techniques have yet to be tested.[35] Here we demonstrate the proof-of-concept of local deposition of surfactant-templated sol−gel silica using a scanning electrochemical microscope. Electro-assisted generation of templated sol−gel films has been previously reported,[30,36,51] but not yet at the local scale.

Scanning electrochemical microscopy (SECM) is now widely recognized as a useful tool for surface modification, with effective ability to micro- and nanopatterning or electrochemical micromachining.[52−54] It takes advantage of the confinement of electron transfer reactions to a small area of a support when an ultramicroelectrode (i.e., micrometer size or less) is brought near its surface. Local modification of substrates by electrochemically generated reagents has been notably exploited for, e.g., electrochemical etching of metals,[55] electro-oxidative lithography,[56] patterning of surfaces with organic or biological molecules,[57] as well as high-resolution electrodeposition of various compounds such as metals,[58−60] conducting polymers,[60−62] organic or biological molecules,[63,64] organometallic derivatives,[65] or inorganic materials.[66−68] Very recently, the local modification of surfaces with sol−gel by SECM has been described,[69] but to date the method was not applied to the surface patterning with mesostructured materials.

■ EXPERIMENTAL SECTION

Electrochemically Assisted Deposition of Silica Microdots. Deposition was made from a starting sol consisting of typically 20 mL ethanol (95−96%, Merck), 20 mL aqueous solution of 0.1 mol L^{-1} $NaNO_3$ (99%, Fluka), 340 mmol L^{-1} tetraethoxysilane (TEOS, 98%, Alfa Aesar), 109 mmol L^{-1} cetyltrimethylammonium bromide (CTAB, 99%, Acros), and a suitable amount of 0.1 M HCl (37%, Riedel de Haen) to reach pH 3. The sol solution was allowed to hydrolyze for one hour prior to use. It was then introduced in a homemade electrochemical cell at the bottom of which the substrate (i.e., ITO plate (surface resistivity 8−12 Ω/sq, Delta Technologies), gold, glassy carbon, or glass) was placed horizontally.

For silica microdots deposition carried out in the tip-generation mode, the working electrode was a Pt ultramicroelectrode (UME) disk (diameter: 10, 25, or 50 μm) while a stainless steel counter-electrode and a AgCl-coated silver wire pseudoreference electrode completed the device. The UME tip was positioned at a distance from the substrate of about 2 thirds of the electrode radius and a cathodic potential of −1.1 V was applied for a selected duration time (2 s, unless stated otherwise) in order to generate the necessary hydroxyl ions to induce polycondensation of the silica precursors. In the goal to deposit a large number of microdots in a successive and reproducible way, an automated cleaning step of the UME surface between each deposition was applied thanks to a robust and fine positioning of the UME using a shearforce control. The general procedure consists in removing the tip from the sol solution after microdot deposition, transferring it in an etchant solution (5% HF, from Prolabo) to

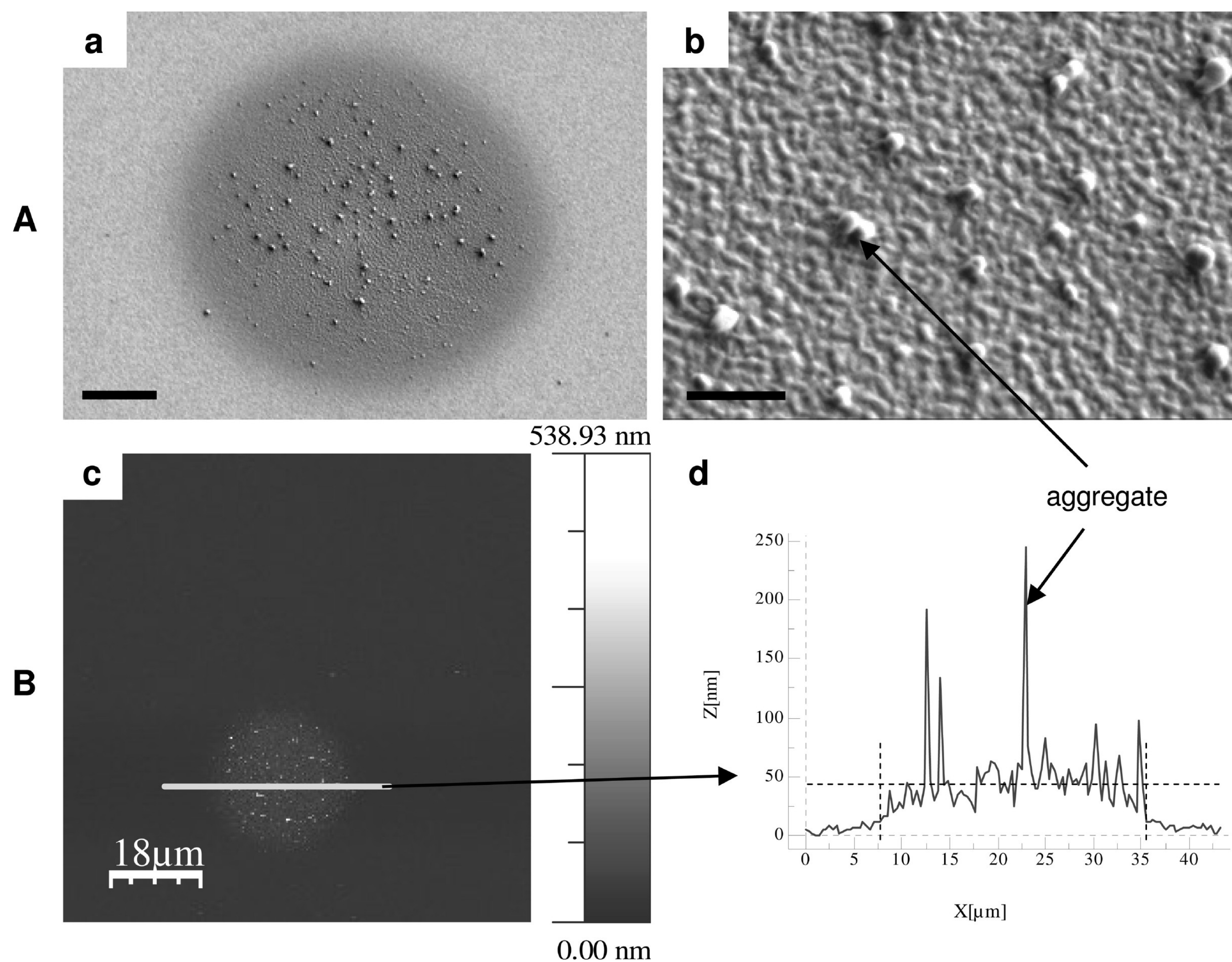

Figure 2. (A) SEM and (B) AFM images of a surfactant-templated silica microdot electrodeposited on ITO. (a) Low- and (b) high-magnification FE-SEM top views of a sample prepared using a 25 μm diameter Pt UME (SECM tip) immersed in a 340 mM TEOS solution containing a CTAB content adjusted to reach $[n_{CTAB}/(n_{TEOS})] = 0.32$. Scale bars correspond to (a) 5 and (b) 1 μm. (c) AFM image of the same microdot, and (d) AFM profile on a line crossing the sample as shown in part c. Other conditions: 2 s electrodeposition using the Pt tip positioned at 10 μm from the ITO surface and biased at $E_{tip} = -1.10$ V.

remove any silica deposit on the UME surface, then to a water bath to wash the UME surface prior to the accurate repositioning of the tip at a desired distance close to the substrate in the sol solution to perform a new deposition step. The experimental procedure used in the "indirect mode" consists in using the UME tip as the counter-electrode and the substrate as the working electrode. This latter is biased at a constant potential value just below the open circuit potential ($E_{substrate} = E_{i=0} - [1\text{ mV}]$) for selected deposition times (typically in the 2−5 s range). After microdots deposition, the substrate was quickly removed from the solution and immediately rinsed with pure water to prevent any formation of an unwanted silica layer by evaporation. The deposits were finally dried and aged overnight in an oven at 130 °C. When necessary, extraction of the surfactant template was made by calcination (at 450 °C for 15 min).

Apparatus. A home-built SECM instrument equipped with a shearforce detection positioning system and a bipotentiostat (PalmSens) was used for microdots deposition as well as to probe the patterned silica thin deposits via electrochemical imaging of conductive and isolating parts of the modified surface. Local variations of electroactivity were revealed by feedback imaging of dried films using $Ru(NH_3)_6^{3+}$ (5 mmol L^{-1}) as the redox probe (in 0.05 mol L^{-1} potassium hydrogen phthalate at pH 4, prepared with high purity water (18 MΩ cm^{-1}) from a Millipore milli-Q water purification system) with a carbon fiber tip (5-μm in diameter) maintained at a constant distance ($z = 2$ μm) from the sample surface. The tip was held at a potential likely to reduce the redox probe (−400 mV) and the feedback current was recorded versus the tip location in the $x-y$ plane. The motor position and data acquisition were controlled by modified software initially developed by Sensolytics (Bochum, Germany).

Various physicochemical techniques have been used to characterize the structure, morphology and thickness of the microdots. The morphology of the deposits was characterized by field-emission scanning electron microscopy (FE-SEM) using a S-4800 Microscope (Hitachi) having a 2.0 nm maximum resolution. Contact-mode atomic force microscopy (AFM) was used to check the thickness and topography of some deposits by using a commercial microscope (MFP-3D-BIO Atomic Force Microscope, Asylum Research), using V-shaped silicon nitride tips (ref MLCT-EXMT-BF, Veeco Instruments) with a spring constant of 0.1 N m^{-1} (manufacturer specifications). The mesostructure of the microdots was evaluated by transmission electron microscopy using a Philips CM20 microscope at an acceleration voltage of 200 kV. The samples were prepared by mechanically removing of some (pieces of) microdots, which were then supported on a carbon-coated copper grid. Numerous pieces of microdots were analyzed in order to check the existence of the mesostructure and pore orientation over large fractions of the deposited material.

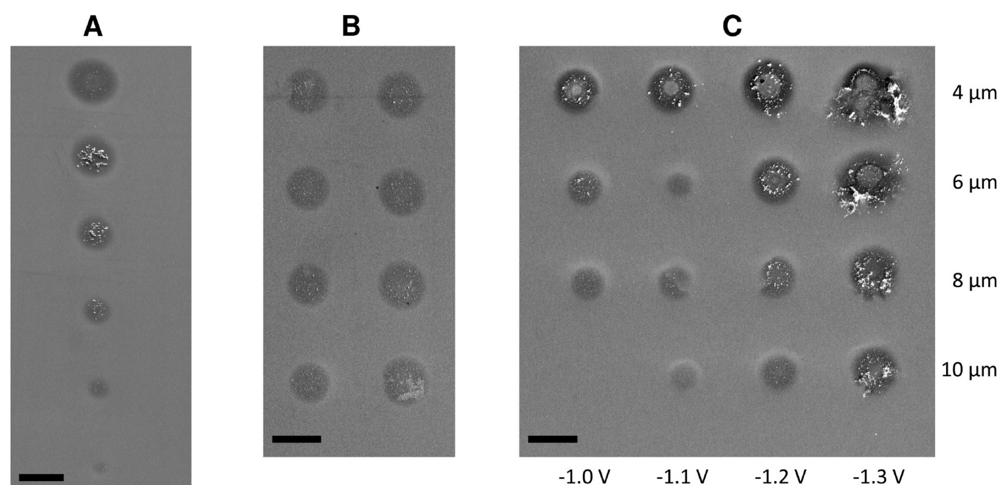

Figure 3. SEM images of surfactant-templated silica microdots formed on ITO by the SECM tip generation mode. (A) Six successive microdots formed in the same conditions as in Figure 2 without any treatment between each deposition. (B) Eight microdots formed as above but after HF cleaning of the SECM tip after each deposition. (C) Sixteen microdots formed as in B but at various applied potential values (horizontal) and tip–substrate distances (vertical). Scale bars correspond to 50 μm. The automated cleaning procedure of the UME was performed as follow: (1) UME immersion in 4% HF solution for 2 s, (2) transfer to distilled water for 10 s, (3) drying for 2 min in atmosphere. Other experimental conditions as in Figure 2.

RESULTS AND DISCUSSION

General Considerations. We show here how SECM integrating a fine nonelectrochemical positioning system is likely to generate local deposits of surfactant-templated mesoporous silica. The method is based on an accurate positioning of an ultramicroelectrode (UME) close to a solid support, which was immersed into a surfactant-containing hydrolyzed sol solution. The tip electrode was then used as a micrometric "pen" inducing self-assembly polycondensation of the precursors by local pH change under potential control. Electro-assisted deposition can occur in two distinct modes (Figure 1): (mode 1) a tip-generation approach in which the hydroxyl ion catalysts are electrogenerated at the SECM tip, and (mode 2) an "indirect mode" relying on the use of the SECM tip as a microscopic auxiliary electrode, which constraints the current lines near the underlying (conductive) substrate that acts as a "local" working electrode. The concept is new and strategically distinct from other lithographic approaches as the mechanisms for inorganic wall construction and amphiphilic assemblies are dominated by potential-controlled sol–gel polycondensation (i.e., different from those of evaporation methods or postsynthesis treatments). As a result, it offers new possibilities to produce patterned mesoporous films that cannot be produced by other means (e.g., microdots with vertically oriented mesopores, which can be obtained in the "indirect mode", as described in the last part of this paper).

Mode 1: "Direct" Tip Generation. The SECM tip is an UME disk with a radius smaller than the diffusion layer thickness achieved in most conventional electrochemical experiments. When an UME is immersed in a solution containing an electrolyte and redox active species, and biased at a suitable potential likely to oxidize (reduce) these species (as in SECM), the observed currents rapidly reach a steady-state value resulting from a constant flux of redox active species driven by an essentially hemispherical diffusion layer around the electrode. Approaching the UME within a few tip diameters of a surface thus induces perturbation of the UME current, which constitutes the basis of the "classical" SECM response, which was notably used to position the tip at a certain distance of the substrate or as imaging tool.[70] In the present case, however, the SECM tip is intended to generate OH^- species in a hemispherical region on the tip surface in order to increase pH locally on a small part of the underlying substrate. A prerequisite to successful film deposition is the fine and controlled positioning of the tip at a selected distance from the substrate so that the hemisphere containing OH^- species partly covers a spherical area where the film is expected to be formed (Figure 1A). This has been achieved here with the aid of a non-optical shearforce detection system integrated in the SECM, which provided a current-independent tip–surface distance positioning (see Figure SI1 in Supporting Information for details). In such conditions, microdots of surfactant-templated silica can be obtained on various supports, conducting or not (indium–tin oxide, gold, glass), from precursor solutions containing prehydrolyzed tetraethoxysilane (TEOS) and cetyltrimethylammonium bromide (CTAB), at pH 3, by applying a suitable cathodic potential (typically −1.1 V) at the platinum UME tip (25 μm in diameter). This induces a pH increase between the macroscopic support and the much smaller SECM tip as a consequence of protons and water reduction,[65] resulting in self-assembly polycondensation of the sol and concomitant film deposition as a microdot onto the underlying surface. The microscopic examination by scanning electron microscopy (SEM, see Figure 2A) or by atomic force microscopy (AFM, see Figure 2B) confirms the presence of a deposit in the form of a thin microdot with a diameter of the same order of magnitude as that of the UME size. Consistent with the electro-assisted deposition of functionalized sol–gel and/or ordered mesoporous silica films onto large supports,[30,34,51,71] the morphology of the deposit reveals the presence of particles (aggregates) in addition to the thin film (average thickness of about 40 nm). These particles are formed because the polycondensation catalyst (OH^-) is electrogenerated in the whole region located between the SECM tip and the underlying surface, a region where gelification occurs as in bulk solution-phase, while preferential deposition as a thin layer on the support was always observed in agreement with

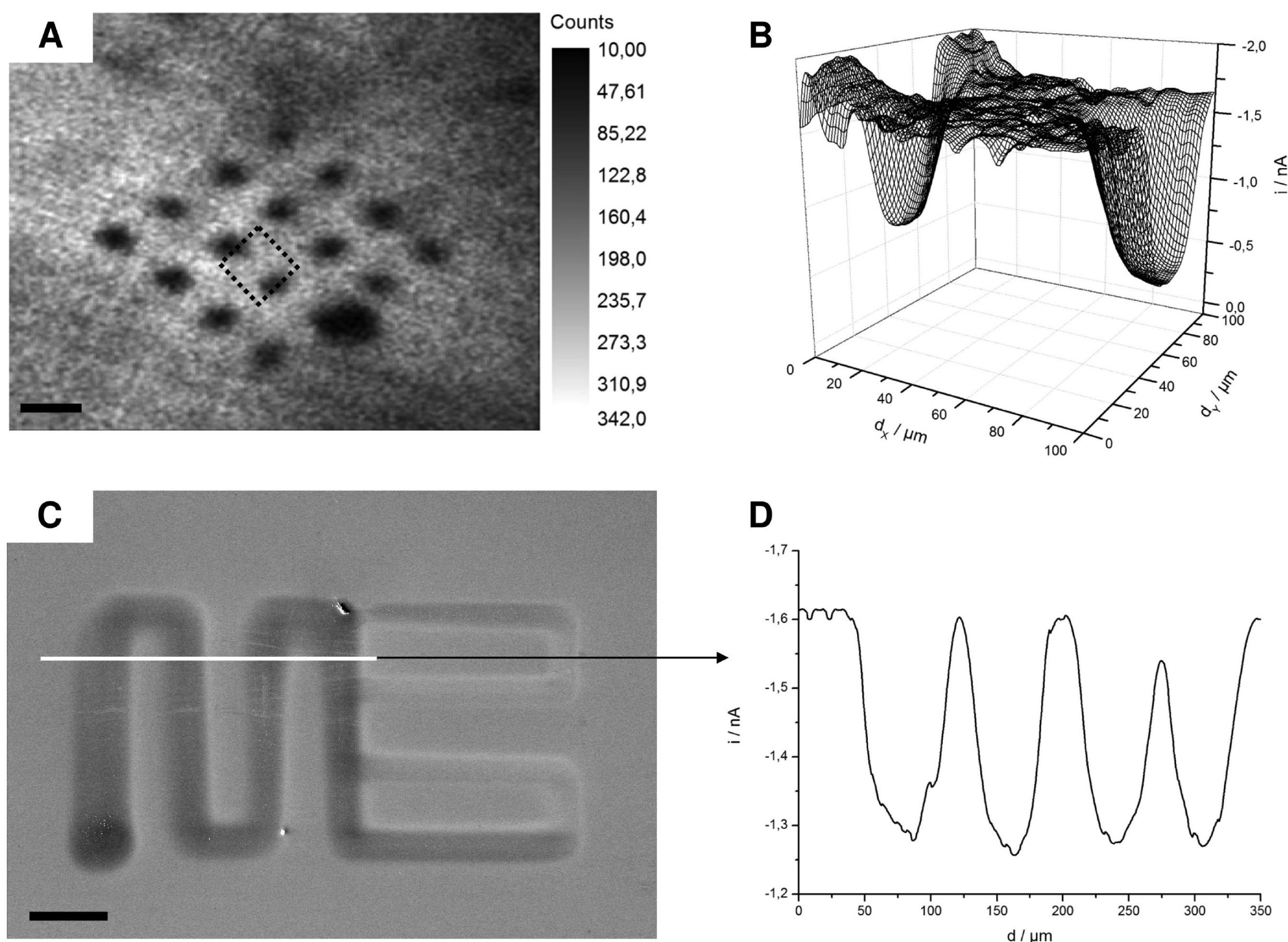

Figure 4. Imaging of surfactant-templated silica patterns by various techniques. (A) XPS imaging at the In_{3d} line (444.7 eV) of 16 microdots prepared as in Figure 3B. (B) SECM feedback imaging of two half microdots (corresponding to the square region in part A using $Ru(NH_3)_6^{3+}$ as the redox probe and a carbon fiber UME tip biased at −400 mV, by recording the feedback current while using the tip to scan a square plane of 100 × 100 μm^2. (C) SEM image of a silica pattern obtained by moving the UME tip (at 15 $\mu m\ s^{-1}$) in the x−y plane. (D) SECM profiles recorded in the same conditions as B along a selected line on the sample depicted in C. Scale bars correspond to 100 μm.

mesoporous silica film formation on (macroscopic) solid surfaces from alkaline solutions.[72,73] Note that Figure 2 just demonstrates the feasibility of the local sol−gel electrodeposition and a detailed study of all parameters affecting this process is mandatory to define the optimal conditions leading to reproducible deposits with controlled characteristics.

The first observation was a significant decrease in the microdot diameter upon successive deposition of several microdots using the same SECM tip which was simply shifted from one place to another one on the x-axis (Figure 3A), the tip−surface distance being readjusted at its selected initial value between each spot by shearforce positioning (useful because the underlying substrate is difficult to be maintained perfectly horizontal over millimetric distances with a deviation less than 1 μm). Such variation is of course not acceptable as far as reproducible patterning is concerned. It results from some "unwanted aging" of the SECM tip due to the growth of a sol−gel layer onto the UME surface (in addition to microdot formation on the underlying substrate), consistent with observations made on larger electrodes biased at negative potentials.[51,71] The unwanted layer, expected to be thicker and thicker in multiple experiments, thus contributes to restrict more and more the effectiveness of OH^- generation and subsequent microdot formation (the amount of deposited matter in multiple successive deposition became lower and lower and microdots smaller and smaller, Figure 3A). It is thus necessary to renew the UME tip surface between each deposit. This can be effectively made by mechanical polishing, leading to reproducible microdots deposition, but this approach is time-consuming and not really relevant to automatic patterning (as the UME has to be manually removed from the SECM device, polished elsewhere, and mounted again on the system). Electrochemical and chemical cleaning procedures, which are compatible with automation via the positioning system of the SECM apparatus, have been thus tested. Without going into details, one can state that in situ electrochemical treatments (e.g., applying low or high overvoltages or potential scans to the UME tip far from the underlying substrate), though giving rise to some improvement with respect to Figure 3A, were not totally satisfactory. The best results were obtained with chemical etching of the sol−gel layer by immersing the UME tip into a diluted HF solution (5%) between each microdot deposition (see Figure 3B for 8 microdots). This can be achieved by programming an automated procedure of the SECM setup, with optimum conditions as follow: microdot electrodeposition − tip immersion in HF for 2 s − washing

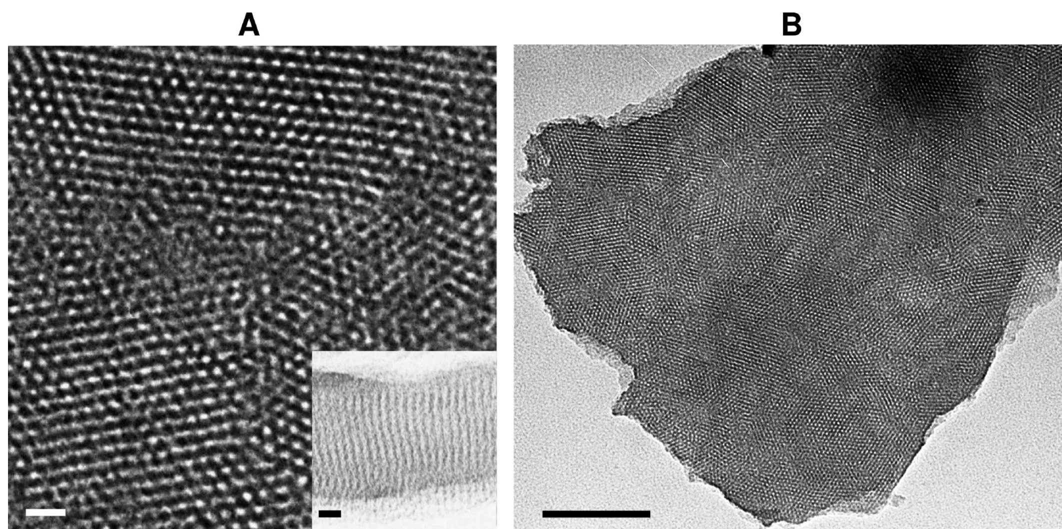

Figure 5. TEM images of surfactant-templated silica microdots formed by the SECM "indirect mode": (A) top view and cross-sectional view as inset; (B) top view of an extended area. These films were electrogenerated for 5 s with the aid of a 25-μm-diameter Pt UME biased at −1 mV vs the open circuit potential and positioned at a distance of 25 μm from an ITO substrate, from sol solutions containing 340 mM TEOS and a CTAB content adjusted to reach $[n_{CTAB}/(n_{TEOS})] = 0.32$. Scale bars correspond to (A) 10 or (B) 100 nm.

with water – drying in air – repositioning of the tip close to the substrate by shearforce control and starting for a new deposit (see details in Experimental Section). The microdots can be also observed with an optical microscope (see Figure SI2 in the Supporting Information). The presence of silica microdots was further evidenced by X-ray Photoelectron Spectroscopy imaging (along the In_{3d} line at 444.7 eV) and the obtained results (see Figure 4A for 16 microdots) clearly show dark spots indicating the local coverage of the indium–tin-oxide support (In_{3d} signal not detectable under the silica microdots). The microdots depicted in Figures 3B and 4A have been prepared on ITO but the versatility of the method enables their formation on various substrates, conducting or not (we have tested gold, platinum, carbon, but also glass), onto which silica microdots can be easily deposited with the aid of the SECM tip biased at a cathodic potential.

Various parameters are likely to affect the localized deposition process, which can be adjusted to control the final characteristics of microdots: the applied potential, the distance between the UME tip and the underlying substrate, the electrodeposition time, and the UME diameter. Figure 3C illustrates the effect of the two first parameters. Consistent with previous investigations on electro-assisted deposition of sol–gel films (mesostructured or not) on large supports,[30,71,74] increasing the cathodic potential led to thicker deposits with larger amounts of aggregates (see horizontal lines in Figure 3C), which is explained by larger amounts of OH^- catalysts generated at the UME surface when applying more negative potential values. Note that the 16 deposits depicted in Figure 3C have been obtained in a single (programmed) experiment, pointing out the interest of the electrochemical patterning method for rapid multiparameter screening (contrary to other lithographic techniques). Controlling the distance between the UME tip and the underlying substrate was likely to tune both the microdot morphology and thickness as a result of the hemispherical OH^- concentration gradient existing at the UME-solution interface (schematically represented in Figure SI3 in the Supporting Information): the distance ensuring the formation of uniform microdots was about one-third of the UME diameter (i.e., 10 μm for a 25 μm sized UME), while much thinner (or no) deposits were observed at longer distances (less OH^- species produced at the vicinity of the underlying substrate) and much thicker and ring-shaped deposits when approaching the UME tip closer to the substrate because of larger OH^- concentrations especially on the external borders of the UME. This underlines the major importance of controlling finely the tip-to-substrate distance, which can be accurately achieved by the shearforce positioning SECM system used here. Evidently, varying the UME size (and adjusting the distance between the UME tip and the substrate at the optimal value of about one-third of its diameter in each case) allowed tuning the diameter of the microdots at values directly proportional to the UME tip diameter (see Figure SI4 in the Supporting Information). Finally, increasing deposition times resulted in increasing the amount of electrogenerated OH^- catalysts and, thereby, to much thicker deposits that became progressively ring-shaped and wider (see Figure SI5 in the Supporting Information) due to the particular OH^- concentration gradients, as discussed above.

These surfactant-templated silica microdots are electrically isolating and not permeable to solution-phase reagents (prior to surfactant extraction, of course), as demonstrated by SECM imaging (see Figure 4B for two half microdots). Indeed, SECM can be used not only for microdots formation but also for distinguishing between conducting and isolating surfaces[53] as well as for the characterization of the permeability properties of an insulating layer (e.g., mesoporous silica) deposited onto a conductive surface (e.g., electrode surface).[75] Using a redox probe in solution (i.e., 5 mmol L^{-1} $Ru(NH_3)_6^{3+}$ in 0.05 mol L^{-1} potassium hydrogen phthalate at pH 4, in this case) and a carbon fiber tip (5 μm in diameter, i.e., 1 order of magnitude smaller than the microdot size) maintained at a constant distance from the substrate bearing the microdots (2 μm in this case), a large cathodic current was observed when the tip was facing the conductive ITO surface (because the redox probes are constantly regenerated at the substrate) whereas only reduction of the probe on UME can occur when the tip was facing the isolating silica microdot (see Figure SI6 in the

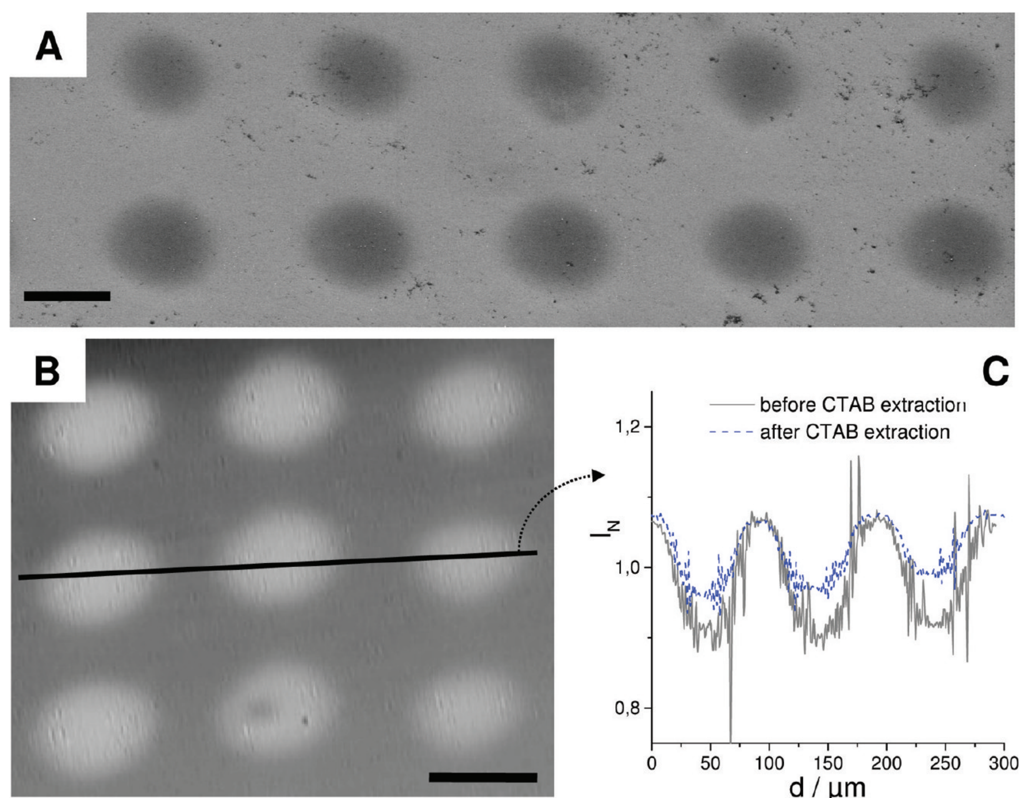

Figure 6. (A) SEM and (B) SECM imaging of surfactant-templated silica microdots formed by the SECM "indirect mode" on ITO. (A) SEM top views of 10 successive microdots electrogenerated for 2 s from a sol solution containing 100 mM TEOS (other conditions as in Figure 5) without any treatment between each deposition step. (B) SECM feedback imaging of a series of 9 microdots, performed in the same conditions as for Figure 4B. (C) SECM profiles (normalized currents with respect to the UME response far from the substrate surface) recorded along the selected line depicted in B, respectively, before and after template extraction. Scale bar corresponds to 50 μm.

Supporting Information for schematic explanation). These data underline the interest of the local electrogeneration method to pattern isolating layers onto conducting substrates, with possible applications in, e.g., microelectronics. An illustrative example is shown in Figure 4C, along with selected SECM lines (Figure 4D) highlighting the succession of insulating and conducting microdomains. The SECM results not only prove that something was deposited, but also that the films are not permeable to the redox probes, suggesting uniform deposits without significant cracks/defects over the whole microdot surface (cracks or defects would have resulted in positive feedback).

Mode 2: "Indirect" Generation. One of the most intriguing tasks in the synthesis of mesoporous thin films is the vertical alignment of the pores as potential applications of such deposits rely on the ability to form films with accessible pores from the surface.[24] To date, alignment of a hexagonal mesostructure in a direction perpendicular to the substrate in patterned mesoporous films was not yet achieved. Unfortunately, the surfactant-templated silica microdots prepared using the tip-generation mode (OH^- catalysts electrogenerated at the SECM tip) were poorly ordered (see Figure SI7 in the Supporting Information), without preferential alignment of mesopores, unless electrochemistry was reported to be an effective way to grow vertically aligned mesopore channels on macroscopic supports.[30] Actually, getting ordered and oriented mesoporous silica thin microdots has required the application of an "indirect mode" based on the use of the SECM tip as a microscopic auxiliary electrode and the underlying substrate acted as a local working electrode when the UME was approached close to itself (see right bottom in Figure 1). In that configuration, local surfactant self-assembly under potential control[76] and electrochemically induced polycondensation of precursors resulted in local growing of well-ordered silica mesochannels perpendicular to the substrate (Figure 5). Even if the observation of such samples by high-resolution TEM has proven to be technically difficult because of their small size and the necessity to mechanically remove the microdots from the substrate, the top view unambiguously shows the regular hexagonal arrangement of mesopores (see part A in Figure 5), over wide areas (see part B in Figure 5) and reproducibly on the basis of multiple TEM analyses of various samples, supporting the idea of uniform deposition over the whole microdot surface areas. In addition, the cross-sectional view (inset in Figure 5A) clearly demonstrates the uniform morphology of the microdot with packed mesochannels oriented normal to the microdot plan. The fact that the "indirect mode" gave rise to oriented mesostructures, while the tip generation one did not, demonstrates the essential role of the substrate polarization on surfactant self-assembly in a form (probably hemimicelles[77]) inducing silica microdots formation from mesopore channels growing perpendicular to the substrate.

The "indirect mode" can be basically applied using either potentiostatic or galvanostatic conditions. Potentiostatic deposition requires the application (to the substrate) of a potential slightly lower than the open circuit potential (typically 1 mV is enough), generating thereby a transient capacitive

current (about −1 μA for some milli-seconds) followed by a plateau current corresponding to the electro-assisted deposition process (e.g., plateau current close to −100 nA for 2 s deposition with a tip−substrate distance of 25 μm). The second approach (application of a current between the UME tip and the underlying substrate) is even much easier because of the very big difference between electrode surface areas (μm^2 range for UME and cm^2 range for the substrate). Typically, this can be achieved by applying a short current pulse (i.e., −1 μA for 10 ms to charge the double layer capacity at the large substrate surface) followed by a plateau current of lower intensity (i.e., −100 nA for an UME of 25 μm in diameter) for deposition to take place. In both cases, the microdot thickness and size are easily controlled, respectively by varying the electrodeposition time and by tuning the UME diameter, similarly as for the tip generation mode (Figure 3C and Figure SI5 in the Supporting Information). For instance, microdot thicknesses in the range 20−50 nm can be obtained by tuning the deposition time between 2 and 5 s.

Interestingly, the "indirect mode" was likely to produce patterns of several microdots by successive deposition without any "aging" effect neither any additional renewal treatment between each microdot formation (see Figure 6A for 10 successive microdots). This attractive feature with respect to automatic micropatterning over wide surfaces is explained by the fact that OH^- catalysts are formed directly on the substrate surface and the redox process involved at the SECM tip (water oxidation into molecular oxygen) does not induce any UME fouling effect. Again, full coverage of the underlying substrate by the surfactant-templated mesoporous silica over the whole microdot surface area can be evidenced by SECM imaging (Figure 6B), giving rise to current profiles (see, e.g., curve a in Figure 6C) indicating succession of conducting and isolating regions. After surfactant extraction, these profiles were significantly different (see, e.g., curve b in Figure 6C) because molecular transport of the probe across the oriented mesoporous silica microdots was effective, thus permitting the probe regeneration at the underlying conducting substrate and increasing locally the reversible kinetic character of these local patterned area. A more detailed explanation of this behavior is also given in Figure SI6 in the Supporting Information. One has to remind here that SECM characterization was made using an UME tip smaller by 1 order of magnitude than the microdot size, in order to be able to evaluate the permeability properties over the whole region of deposition. A further control experiment to support this claim is illustrated in Figure SI8 in the Supporting Information, mimicking the situation of Figure 6, but at a larger scale. Indeed, a homogeneous oriented mesoporous film (hexagonal mesostructure and pore orientation proved by grazing incidence X-ray diffraction), which was partly removed (mm scale) using HF drops without damaging the underlying ITO substrate, gave rise to the same SECM profiles as in Figure 6C before and after surfactant extraction. This result indicates thereby that SECM is the relevant technique, yet indirect, to analyze the permeability of patterned mesoporous silica dots. In a situation where other techniques currently employed for assessing the pore orientation (grazing incidence X-ray diffraction) or the porosity (gas adsorption) of mesoporous thin films failed because of too small quantity of material in microdots, the SECM data given here for individual microdots (which are similar to those obtained with larger oriented mesoporous films intentionally damaged at the mm scale; compare Figure 6C with Figure SI8 in the Supporting Information), along with TEM data (Figure 5), support the idea of uniform mesoporous deposits (i.e., deposits exhibiting homogeneous permeabilities owing to a homogeneous quality of their mesostructures) without significant cracks/defects over the whole microdot surface.

■ CONCLUSIONS AND PROSPECTS

Formation of surfactant-templated silica microdots by SECM constitutes a conceptual novelty with respect to the previously reported patterning techniques used to grow mesoporous silica films on a microscopic scale. The approach can be used in both tip generation and "indirect" modes to generate isolating patterns on conducting substrates. Microdots of well-ordered mesostructures with unprecedented vertical orientation of mesopore channels can be obtained in a reproducible way using the "indirect" mode (UME as auxiliary electrode) without requiring any treatment of the SECM tip between each deposition event. Such oriented mesostructuration is highly recommended for practical applications requiring enhanced accessibility and fast mass transport issues. They could find interest in various domains, such as microfluidics, lab-on-a-chip manufacturing, micro-optics or micro(spectro)electrochemical devices development. A recent report showed that locally deposited mesoporous materials provide additional properties to the underlying surface, for example to promote the adsorption of chemical species and/or for nanofluidics applications.[78] The novel method is intended to have broad interests as the nonelectrochemical fine positioning system based on shearforce control is compatible with patterning of non flat surfaces and the versatility of electrochemically induced sol−gel processing can be exploited to prepare organically functionalized nanocomposites or to generate metal oxide coatings other than silica, or even to pattern any other kind of materials which can be deposited by electro-induced pH changes (as, for example, organic polymers or metal hydroxides). Finally, the resort to nanoelectrodes (they can be fabricated nowadays with diameters down to 10 nm) would open the way to nanopatterning of such mesoporous structures, with promising avenues in the land of nanochemistry.[79]

■ ASSOCIATED CONTENT

Supporting Information

Additional figures (PDF). This material is available free of charge via the Internet at http://pubs.acs.org.

■ AUTHOR INFORMATION

Corresponding Author

*Tel.: (+33) 3 83 68 52 59. Fax: (+33) 3 83 27 54 44. E-mail: alain.walcarius@lcpme.cnrs-nancy.fr.

■ ACKNOWLEDGMENTS

We are grateful to J. Ghanbaja, L. Mouton, and A. Renard for TEM, FE-SEM and XPS experiments, respectively.

■ REFERENCES

(1) Kresge, C. T.; Leonowicz, M. E.; Roth, W. J.; Vartuli, J. C.; Beck, J. S. *Nature* **1992**, *359*, 710−712.

(2) Wan, Y.; Zhao, D. *Chem. Rev.* **2007**, *107*, 2821−2860.

(3) Hoffmann, F.; Cornelius, M.; Morell, J.; Froeba, M. *Angew. Chem., Int. Ed.* **2006**, *45*, 3216−3251.

(4) Sanchez, C.; Rozes, L.; Ribot, F.; Laberty-Robert, C.; Grosso, D.; Sassoye, C.; Boissiere, C.; Nicole, L. *C. R. Chim.* **2010**, *13*, 3−39.

(5) Hartmann, M. *Chem. Mater.* **2005**, *17*, 4577−4593.
(6) Clark, J. H.; MacQuarrie, D. J.; Tavener, S. J. *Dalton Trans.* **2006**, 4297−4309.
(7) Slowing, I. I.; Trewyn, B. G.; Giri, S.; Lin, V.S.-Y. *Adv. Funct. Mater.* **2007**, *17*, 1225−1236.
(8) Klichko, Y.; Liong, M.; Choi, E.; Angelos, S.; Nel, A. E.; Stoddart, J. F.; Tamanoi, F.; Zink, J. I. *J. Am. Ceram. Soc.* **2008**, *92*, S2−S10.
(9) Vallet-Regi, M. *J. Intern. Med.* **2009**, *267*, 22−43.
(10) Walcarius, A.; Mercier, L. *J. Mater. Chem.* **2010**, *20*, 4478−4511.
(11) Nicole, L.; Boissière, C.; Grosso, D.; Quach, A.; Sanchez, C. *J. Mater. Chem.* **2005**, *15*, 3598−3627.
(12) Chao, K.-J.; Liu, P.-H.; Huang, K.-Y. *C. R. Chim.* **2005**, *8*, 727−739.
(13) Penard, A.-L.; Gacoin, T.; Boilot, J.-P. *Acc. Chem. Res.* **2007**, *40*, 895−902.
(14) Sanchez, C.; Boissière, C.; Grosso, D.; Laberty, C.; Nicole, L. *Chem. Mater.* **2008**, *20*, 682−737.
(15) Walcarius, A.; Kuhn, A. *Trends Anal. Chem.* **2008**, *27*, 593−603.
(16) Hu, X.; Li, G.; Yu, J. C. *Langmuir* **2010**, *26*, 3031−3039.
(17) Ogawa, M. *Curr. Top. Colloid Interface Sci.* **2001**, *4*, 209−217.
(18) Lu, Y.; Ganguli, R.; Drewien, C. A.; Anderson, M. T.; Brinker, C. J.; Gong, W.; Guo, Y.; Soyez, H.; Dunn, B.; Huang, M. H.; Zink, J. I. *Nature* **1997**, *389*, 364−368.
(19) Brinker, C. J.; Lu, Y.; Sellinger, A.; Fan, H. *Adv. Mater.* **1999**, *11*, 579−585.
(20) Grosso, D.; Cagnol, F.; Soler-Illia, G.J.D.A.A.; Crepaldi, E. L.; Amenitsch, H.; Brunet-Bruneau, A.; Bourgeois, A.; Sanchez, C. *Adv. Mater.* **2004**, *14*, 309−322.
(21) Smarsly, B.; Fattakhova-Rohlfing, D. Evaporation-induced self-assembly for the preparation of porous metal oxide films. In *Solution Processing of Inorganic Materials*; Mitzi, D.B., Ed.; John Wiley & Sons: Hoboken, NJ, 2009; Chapter 9, pp 283−312.
(22) Yang, H.; Coombs, N.; Sokolov, I.; Ozin, G. A. *Nature* **1996**, *381*, 589−592.
(23) Yang, H.; Kuperman, A.; Coombs, N.; Mamiche-Afara, S.; Ozin, G. A. *Nature* **1996**, *379*, 703−705.
(24) Brinker, C. J.; Dunphy, D. R. *Curr. Opin. Colloid Interface Sci.* **2006**, *11*, 126−132.
(25) Lee, U.-H.; Kim, M.-H.; Kwon, Y.-U. *Bull. Korean Chem. Soc.* **2006**, *27*, 808−816.
(26) Yamaguchi, A.; Uejo, F.; Yoda, T.; Uchida, T.; Tanamura, Y.; Yamashita, T.; Teramae, N. *Nat. Mater.* **2004**, *3*, 337−341.
(27) Freer, E. M.; Krupp, L. E.; Hinsberg, W. D.; Rice, P. M.; Hedrick, J. L.; Cha, J. N.; Miller, R. D.; Kim, H.-C. *Nano Lett.* **2005**, *5*, 2014−2018.
(28) Yamauchi, Y.; Sawada, M.; Sugiyama, A.; Osaka, T.; Sakka, Y.; Kuroda, K. *J. Mater. Chem.* **2006**, *16*, 3693−3700.
(29) Fukumoto, H.; Nagano, S.; Kawatsuki, N.; Seki, T. *Chem. Mater.* **2006**, *18*, 1226−1234.
(30) Walcarius, A.; Sibottier, E.; Etienne, M.; Ghanbaja, J. *Nat. Mater.* **2007**, *6*, 602−608.
(31) Nagarajan, S.; Li, M.; Pai, R. A.; Bosworth, J. K.; Busch, P.; Smilgies, D.-M.; Ober, C. K.; Russell, T. P.; Watkins, J. J. *Adv. Mater.* **2008**, *20*, 246−251.
(32) Richman, E. K.; Brezesinski, T.; Tolbert, S. H. *Nat. Mater.* **2008**, *7*, 712−717.
(33) Platschek, B.; Koehn, R.; Doeblinger, M.; Bein, T. *ChemPhysChem* **2008**, *9*, 2059−2067.
(34) Etienne, M.; Goux, A.; Sibottier, E.; Walcarius, A. *J. Nanosci. Nanotechnol.* **2009**, *9*, 2398−2406.
(35) Sel, O.; Sallard, S.; Brezesinski, T.; Rathousky, J.; Dunphy, D. R.; Collord, A.; Smarsly, B. M. *Adv. Funct. Mater.* **2007**, *17*, 3241−3250.
(36) Etienne, M.; Sallard, S.; Schröder, M.; Guillemin, Y.; Mascotto, S.; Smarsly, B. M.; Walcarius, A. *Chem. Mater.* **2010**, *22*, 3426−3432.
(37) Innocenzi, P.; Kidchob, T.; Falcaro, P.; Takahashi, M. *Chem. Mater.* **2008**, *20*, 607−614.
(38) Doshi, D. A.; Huesing, I. K.; Lu, M.; Fan, H.; Lu, Y.; Simmons-Potter, K.; Potter, B. G. Jr.; Hurd, A. J.; Brinker, C. J. *Science* **2000**, *290*, 107−111.
(39) Dattelbaum, A. M.; Amweg, M. L.; Ecke, L. E.; Yee, C. K.; Shreve, A. P.; Parikh, A. N. *Nano Lett.* **2003**, *3*, 719−722.
(40) Fan, H.; Lu, Y.; Stump, A.; Reed, S. T.; Baer, T.; Schunk, R.; Perez-Luna, V.; Lopez, G. P.; Brinker, C. J. *Nature* **2000**, *405*, 56−60.
(41) Su, M.; Liu, X.; Li, S.-Y.; Dravid, V. P.; Mirkin, C. A. *J. Am. Chem. Soc.* **2002**, *124*, 1560−1561.
(42) Yang, H.; Coombs, N.; Ozin, G. A. *Adv. Mater.* **1997**, *9*, 811−814.
(43) Hozumi, A.; Kojima, S.; Nagano, S.; Seki, T.; Shirahata, N.; Kameyama, T. *Langmuir* **2007**, *23*, 3265−3272.
(44) Wu, C.-W.; Aoki, T.; Kuwabara, M. *Nanotechnology* **2004**, *15*, 1886−1889.
(45) Hozumi, A.; Kimura, T. *Langmuir* **2008**, *24*, 11141−11146.
(46) Mougenot, M.; Lejeune, M.; Baumard, J. F.; Boissiere, C.; Ribot, F.; Grosso, D.; Sanchez, C.; Noguera, R. *J. Am. Ceram. Soc.* **2006**, *89*, 1876−1882.
(47) Yang, P.; Wirnsberger, G.; Huang, H. C.; Cordero, S. R.; McGehee, M. D.; Scott, B.; Deng, T.; Whitesides, G. M.; Chmelka, B. F.; Buratto, S. K.; Stucky, G. D. *Science* **2000**, *287*, 465−467.
(48) Pai, R. A.; Humayun, R.; Schulberg, M. T.; Sengupta, A.; Sun, J.-N.; Watkins, J. J. *Science* **2004**, *303*, 507−511.
(49) Su, B.; Lu, X.; Lu, Q.; Li, X.; You, C.; Jia, J. *Chem. Mater.* **2009**, *21*, 4970−4976.
(50) Pang, J.; Stuecker, J. N.; Jiang, Y.; Bhakta, A. J.; Branson, E. D.; Li, P.; Cesarano, J. III; Sutton, D.; Calvert, P.; Brinker, C. J. *Small* **2008**, *4*, 982−989.
(51) Goux, A.; Etienne, M.; Aubert, E.; Lecomte, C.; Ghanbaja, J.; Walcarius, A. *Chem. Mater.* **2009**, *21*, 731−741.
(52) Schuster, R.; Kirchner, V.; Allongue, P.; Ertl, G. *Science* **2000**, *289*, 98−101.
(53) Mandler, D. In *Scanning Electrochemical Microscopy*; Bard, A. J., Mirkin, M. V., Eds.; Marcel Dekker: New York, 2001; pp 593−627.
(54) Simeone, F. C.; Albonetti, C.; Cavallini, M. *J. Phys. Chem. C* **2009**, *113*, 18987−18994.
(55) Sheffer, M.; Mandler, D. *J. Electroanal. Chem.* **2008**, *622*, 115−120.
(56) Hoeppener, S.; Schubert, U. S. In *Applied Scanning Probe Methods XIII. Biomimetics and Industrial Applications*; Bhushan, B., Fuchs, H., Eds.; NanoScience and Technology book Series; Springer: Berlin, 2009; pp 45−70.
(57) Turyan, I.; Matsue, T.; Mandler, D. *Anal. Chem.* **2000**, *72*, 3431−3435.
(58) Turyan, I.; Etienne, M.; Mandler, D.; Schuhmann, W. *Electroanalysis* **2005**, *17*, 538−542.
(59) Radtke, V.; Hess, C.; Heinze, J. *Z. Phys. Chem.* **2007**, *221*, 1221−1236.
(60) Lin, J. C.; Chang, T. K.; Yang, J. H.; Chen, Y. S.; Chuang, C. L. *Electrochim. Acta* **2010**, *55*, 1888−1894.
(61) Kranz, C.; Ludwig, M.; Gaub, H. E.; Schuhmann, W. *Adv. Mater.* **1995**, *7*, 38−40.
(62) Kranz, C.; Gaub, H. E.; Schuhmann, W. *Adv. Mater.* **1996**, *8*, 634−637.
(63) Cougnon, C.; Mauzeroll, J.; Bélanger, D. *Angew. Chem., Int. Ed.* **2009**, *48*, 7395−7397.
(64) Chen, P. C.; Chen, R. L. C.; Cheng, T. J.; Wittstock, G. *Electroanalysis* **2009**, *21*, 804−810.
(65) Neufeld, A. K.; O'Mullane, A. P.; Bond, A. M. *J. Am. Chem. Soc.* **2005**, *127*, 13846−13853.
(66) Shohat, I.; Mandler, D. *J. Electrochem. Soc.* **1994**, *141*, 995−999.
(67) Sauter, S.; Wittstock, G. *J. Solid State Electrochem.* **2001**, *5*, 205−211.
(68) Reveron, H.; Elissalde, C.; Lecoutre, C.; Garrabos, Y. *Mater. Lett.* **2008**, *62*, 1067−1070.
(69) Liu, L.; Toledano, R.; Danieli, T.; Zhang, J.-Q.; Hu, J.-M.; Mandler, D. *Chem. Commun.* **2011**, *47*, 6909−6911.
(70) Bard, A. J.; Fan, F. R. F.; Mirkin, M. V. *Electroanal. Chem.* **1994**, *18*, 243−373.
(71) Sibottier, E.; Sayen, S.; Gaboriaud, F.; Walcarius, A. *Langmuir* **2006**, *22*, 8366−8373.

(72) Ogawa, M.; Shimura, N.; Ayral, A. *Chem. Mater.* **2006**, *18*, 1715–1718.
(73) Shimura, N.; Ogawa, M. *J. Colloid Interface Sci.* **2006**, *303*, 250–255.
(74) Shacham, R.; Avnir, D.; Mandler, D. *Adv. Mater.* **1999**, *11*, 384–388.
(75) Guillemin, Y.; Etienne, M.; Aubert, E.; Walcarius, A. *J. Mater. Chem.* **2010**, *20*, 6799–6807.
(76) Choi, K.-S.; McFarland, E. W.; Stucky, G. D. *Adv. Mater.* **2003**, *15*, 2018–2021.
(77) Sanchez-Rivera, A. E.; Vital-Vaquier, V.; Romero-Romo, M.; Ramirez-Silva, M. T.; Palomar-Pardave, M. *J. Electrochem. Soc.* **2004**, *151*, C666–C673.
(78) Faustini, M.; Vayer, M.; Marmiroli, B.; Hillmyer, M.; Amenitsch, H.; Sinturel, C.; Grosso, D. *Chem. Mater.* **2010**, *22*, 5687–5694.
(79) Ozin, G. A.; Arsenault, A. C.; Cademartiri, L. *Nanochemistry: A Chemical Approach to Nanomaterials*, 2nd ed.; The Royal Society of Chemistry: Cambridge, U.K., 2009.